Formability of a non-crimp 3D orthogonal weave E-glass composite reinforcement

Juan Pazmino [a], Valter Carvelli [a,*], Stepan V. Lomov [b]

[a] Department of Architecture, Built Environment and Construction Engineering, Politecnico di Milano, Piazza Leonardo da Vinci 32, 20133 Milan, Italy
[b] Department of Metallurgy and Materials Engineering, KU Leuven, Kasteelpark Arenberg 44, B-3001 Leuven, Belgium

Received 18 November 2013
Received in revised form 4 February 2014
Accepted 5 February 2014
Available online 13 February 2014

1. Introduction

Textile reinforcements for composite structures have attracted lots of attention due to their superior shaping characteristics compared with laminates [1]. Textile reinforcements are especially efficient in manufacturing composite structures with complex shapes. Interlacing of warp and weft yarns allows forming complex shapes without defects that are difficult to obtain with unidirectional reinforcements [2].

During manufacturing process, a crucial step is the forming of flat textile reinforcements into a desired (three-dimensional) shape. The shape of the preform is generally obtained by punch and die draping process. After shaping, the reinforcement is injected with resin and consolidated. Forming of double-curved shapes is a critical phase due to in-plane deformations and above all in-plane shear [3]. The deformability of the reinforcement defines the fibre orientations and density, which influences directly the permeability of the preform, and finally the mechanical response of a composite component. Therefore, the knowledge of the behaviour during forming of a dry composite reinforcement is of primary importance to avoid defects (e.g. wrinkling) in complex preforms and to establish the quality of the manufacturing.

* Corresponding author. Tel.: +39 0223994354.
E-mail address: valter.carvelli@polimi.it (V. Carvelli).

In spite of the fast growing interest for 3D orthogonal interlock woven reinforcements in the composites industry for a broad range of applications [4], the behaviour during forming of these reinforcements are not deeply known and investigated. In fact, most of the studies available in the literature (see e.g. [3,5–8]) are dedicated to forming of textile reinforcements with two-dimensional interlacements. In [9,10] experimental data and numerical modelling are detailed for a specific type of angle interlock carbon fabrics. The authors are not aware of similar studies for orthogonal 3D woven reinforcements. Their behaviour, due to a specific geometry of Z-binding and extreme straightness of the stuffing warp and weft yarns [11,12], is quite different from the tight heavily interlaced angle interlock weaves [13].

In this paper, the formability of a single layer E-glass non-crimp 3D orthogonal woven reinforcement (commercialized under trademark 3WEAVE® by 3Tex Inc.), is experimentally investigated. The study involves the experimental simulation of the forming process on two moulds, i.e. tetrahedral and double-dome shape. The tests are assisted by 3D digital image correlation technique to have a continuous measurement of the local deformation during shaping. Particular attention is dedicated to the in-plane shear deformation distribution, being considered the primary deformation mechanism during shaping [14]. The appearance of wrinkles is also related to the bending stiffness of the textile [3,15]. Therefore, bending tests in warp and weft direction are first presented. Blank

holder is commonly adopted in shaping processes of fabrics with negligible bending stiffness introducing tension in yarns and delaying the out of plane defects. The elevated bending stiffness of the 3D fabric allows excluding blank holders in the forming set-up and delaying the onset of wrinkles in the useful part of the preform.

The present paper continues the study on the deformability of 3D woven fabrics (all done for the same fabric as investigated in this paper), started in [16] with investigation of shear, biaxial tension and compression behaviour of the fabric, continued in [17] with micro-CT observations of change of the fabric internal structure under shear, and in [18] for a comparative analysis of different DIC algorithms for the measurement of fabric 3D deformation.

The experimental results give an important knowledge on the complex double curvature shape formability of the considered 3D fabric composite reinforcement and allow detailed assessment of numerical modelling of these shaping processes. Available numerical modelling based on discrete [19] or continuous [20] approaches can be adopted to predict the forming process of complex shapes assuming the knowledge of the main mechanical features of the 3D textile, as described in Section 4 and in [16], and assessing the accuracy with the experimental forming results presented in Section 5.

2. Non-crimp 3D orthogonal woven reinforcement

The fabric is a single layer E-glass non-crimp 3D orthogonal woven reinforcement (commercialized under trademark 3WEAVE® by 3Tex Inc.). The fibre architecture of the preform has three warp and four weft layers, interlaced by through thickness (*Z*-directional) yarns (Fig. 1 [21]). The fabric construction results in ∼49%/∼49%/∼2% ratio of the fibre amounts (by volume) in the warp, weft and Z fibre directions, respectively. Its thickness, measured by different techniques, is 2.57 ± 0.42 mm (see [17]). The same 3D glass reinforcement was adopted in the composite experimentally investigated in [21–23]. A detailed description of the 3D orthogonal weaving production process is presented in [24,25]. The fibre material is PPG Hybon 2022 E-glass. Some features of the non-crimp 3D reinforcement are listed in Table 1. The reader is referred to [12] for description of the preform architecture, studied with optical microscopy and micro-CT. Furthermore, biaxial tensile and shear mechanical properties of the E-glass non-crimp 3D orthogonal woven reinforcement are detailed in [16].

3. Experimental methods

3.1. Bending tests

In forming processes of textile reinforcements common defects include wrinkles. They develop as a consequence of the low stiffness in some deformation modes of textiles (e.g. in-plane shear and bending) [15]. A common strategy to prevent wrinkles is the addition of forming constraints, such as blank holders, applying tension to fibres.

Bending stiffness of a textile plays an important role in its drapability [26], providing stability to in-plane (shear) deformations [27–29]. An increase of this rigidity leads to an increase of the wrinkle size and a decrease of their number [15].

The measurement of the bending behaviour of the single layer E-glass fabric is detailed in the present work to assess its stiffness in comparison to other reinforcements and to motivate the adopted forming set-up without a blank holder.

Two test methods are known to measure the bending stiffness of fabrics [30]: a cantilever bending test, which originates from the work of Peirce [31] (see [32,2]) and the Kawabata test [33]. In the following, bending tests in warp and weft direction of the 3D reinforcement are detailed using the same type of flexometer as the one developed in [2]. The device consists of a metallic part, which enables to place the sample in cantilever configuration under its own weight (Fig. 2) and an optical device acquiring images of the bent specimen. The quasi-static bending tests with different overhanging lengths allow to measure the non-linear moment vs. curvature relationship. The bending length is increased at steps of 50 mm. After each length increment and before taking image for fixing the deformed configuration, the reinforcement relaxes for five minutes reaching a 'stable' configuration. The image processing generates digital profiles of bent specimens adopted for curvature and moment evaluations, as explained in Section 4. The samples have a full length of 650 mm and a width of 100 mm.

Table 1
Properties of the non-crimp 3D orthogonal weave preform. Data provided by 3Tex Inc. [21].

	Fabric plies	1
	Areal density (g/m^2)	3255
Warp	Insertion density (ends/cm)	2.76
	Top and bottom layer yarns (tex)	2275
	Middle layer yarns (tex)	1100
Weft	Insertion density (ends/cm)	2.64
	Yarns (tex)	1470
Z-yarns	Insertion density (ends/cm)	2.76
	Yarns (tex)	1800

3.2. Forming tests

In order to experimentally study the forming stage for complex double curvature mould shapes, the set-up illustrated in Fig. 3 was

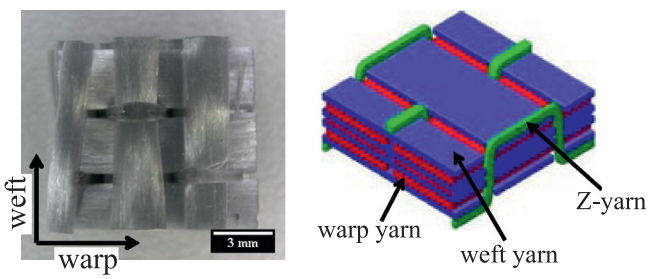

Fig. 1. Architecture of the tows inside the non-crimp 3D orthogonal weave preform [21]: picture (left) and scheme (right) of the unit cell. (For interpretation of the references to colour in this figure legend, the reader is referred to the web version of this article.)

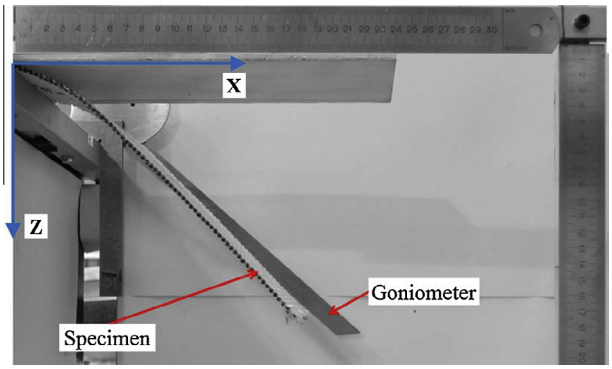

Fig. 2. Bending test set up. (For interpretation of the references to colour in this figure legend, the reader is referred to the web version of this article.)

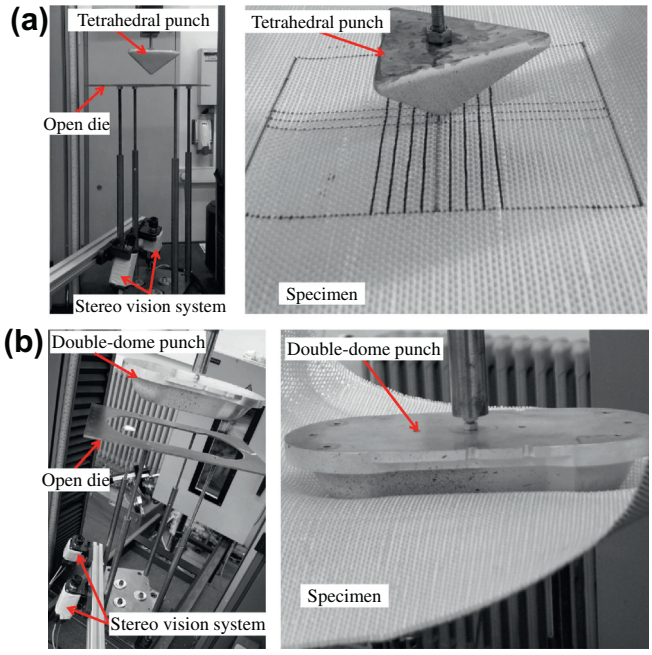

Fig. 3. Forming test set up: (a) tetrahedral shape; (b) double-dome shape. (For interpretation of the references to colour in this figure legend, the reader is referred to the web version of this article.)

prepared. It consists of two modules: a set of metal components and optical devices. The first module is made up of a punch with a complex shape (i.e. tetrahedral and double-dome), and a metal open die on which lies the composite reinforcement. The tetrahedral punch is similar to the one experimentally and numerically investigated for composite reinforcements in [3,34,35]; while the double-dome punch is the one introduced in the benchmark study [36], used in [37] for thermoforming of glass-PP woven fabrics and in [38] for forming behaviour of a non-crimp thermoplastic crossply laminate. The geometry of the metal tools is depicted in Fig. 4. The optical module is a stereo vision system (see Fig. 3), which acquires images of the forming process at a frequency of 1 Hz for 3D image correlation analysis by MatchID3D software [39]. For this purpose the specimen surface is speckled with black and white acrylic paint for displacement measurements with digital image correlation technique [40]. The very thin layer of paint does not change the deformability behaviour of the considered fabric as observed in [16].

A rectangular blank (500 × 600 mm) is placed on the die and a loading cell of 30 kN is adopted to measure the force pushing down the textile at a constant rate of 10 mm/min. The test continues until the forming process is finished, i.e. the punch passes entirely through the die (approximately 65 mm of punch displacement).

Four tests were performed for the tetrahedral shape with warp and weft yarns of the fabric initially aligned to the sides of the rectangular open die (see Figs. 3 and 4). Five specimens were adopted for double-dome forming. Three specimens had the initial direction of the warp and weft yarns parallel to the sides of the die (orientations named 0°/90°), and two specimens with yarns at ±45° to the sides of the die (orientations named ±45°).

4. Bending behaviour

Image post-processing, filtering and binarization allow extraction of the average profiles of the bent specimens for different overhanging lengths L (see Fig. 5). The bent profile of each specimen ($z(x)$) is fitted with a sixth order polynomial function. Each curve in Fig. 5 is the average of three tests. The curvature (κ) in the bent shape is calculated as:

$$\kappa(x) = \frac{Z''}{(1+z'^2)^{\frac{3}{2}}} \tag{1}$$

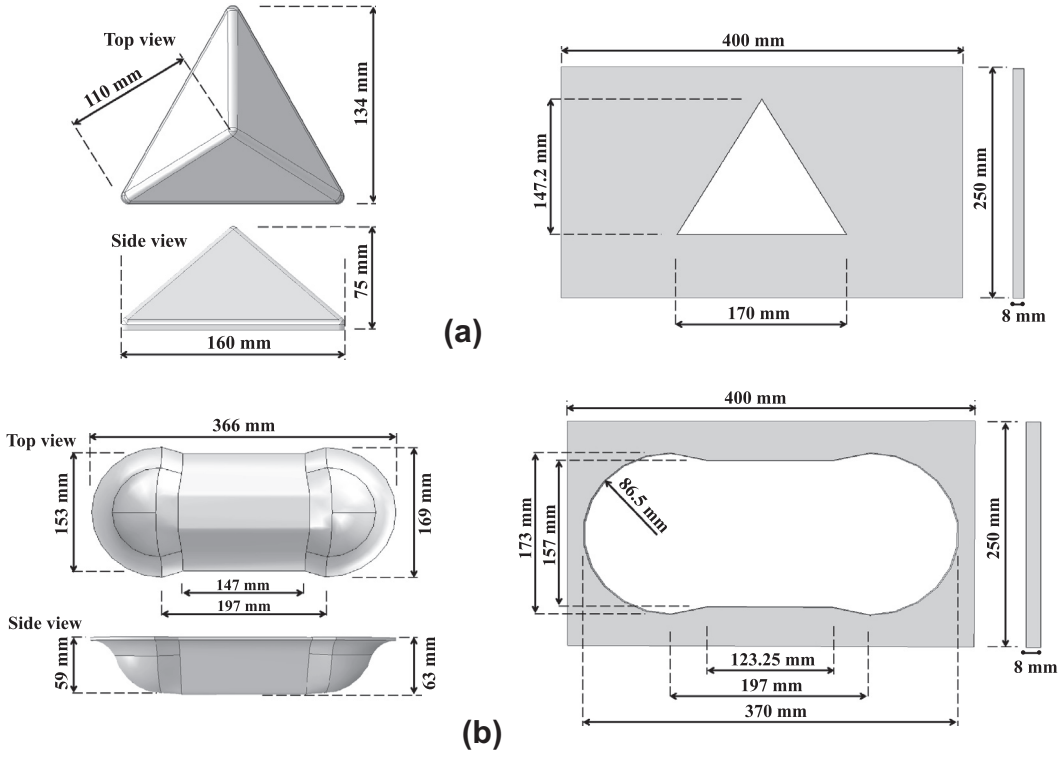

Fig. 4. Forming tools: (a) tetrahedron (left) and open die (right); (b) double-dome (left) and open die (right).

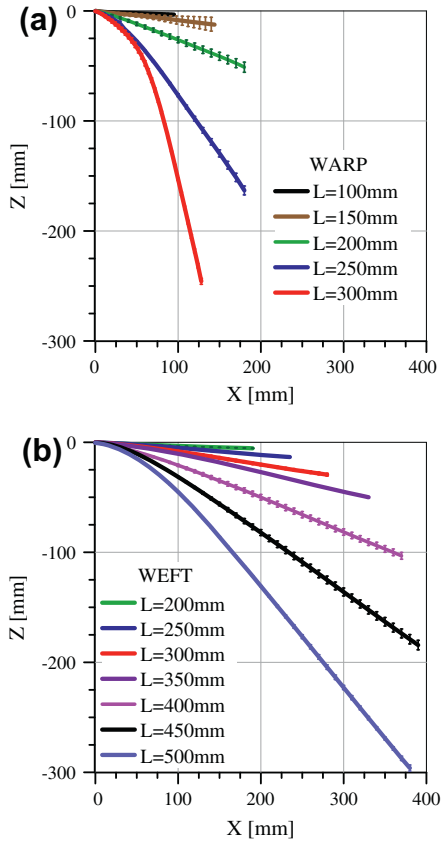

Fig. 5. Sixth order polynomial fitting of bent specimen average profiles extracted by images post-processing for different overhanging length L, in: (a) warp and (b) weft direction. Error bars give the standard deviation of three tests. (For interpretation of the references to colour in this figure legend, the reader is referred to the web version of this article.)

Table 2
Comparison of moment and curvature for the E-glass non-crimp 3D orthogonal woven and two carbon textiles (Fabric A and Fabric B) adopted in [2]).

	Moment per unit width (N)	Curvature (mm^{-1})
Fabric A – weft	0.079	0.037
Fabric B – weft	0.095	0.030
3D – weft	0.59	0.0014
3D – warp	0.58	0.0079

where apex indicates the derivative of the deflection z with respect to the coordinate x (see Fig. 2).

A digital method is adopted to calculate the bending moment. The image of the bent profile is subdivided in segments whose length is about 5 or 10 mm. The weight per unit length and the distance of centroid to the clamp give the contribution of each segment to the bending moment.

The relationships of the curvature (Fig. 6a) and the bending moment (Fig. 6b) at the clamp position with the overhanging length provide the moment–curvature curves depicted in Fig. 6c, as in [2]. These are estimated for overhanging length L in the range 100–300 mm in warp and 200–500 mm in weft direction, respectively.

Fig. 6 shows different bending behaviour of the fabric in the warp and weft directions. This is mainly due to the structure of the reinforcement, made up of three warp and four weft layers (see details in Section 2), even if amounts of the fibres in both directions are the same. The weft outer tows lead to higher bending stiffness of the fabric along this direction.

The bending moment and curvature of the 3D reinforcement and two textiles adopted in [2] (a 2.5D carbon fabric 630 g/m^2 (Fabric A) and an interlock carbon fabric 600 g/m^2 (Fabric B)) are compared in Table 2 for overhanging length L = 200 mm. The comparison of the three textiles with different fibres (glass and carbon) is not completely adequate. But, in the authors' knowledge,

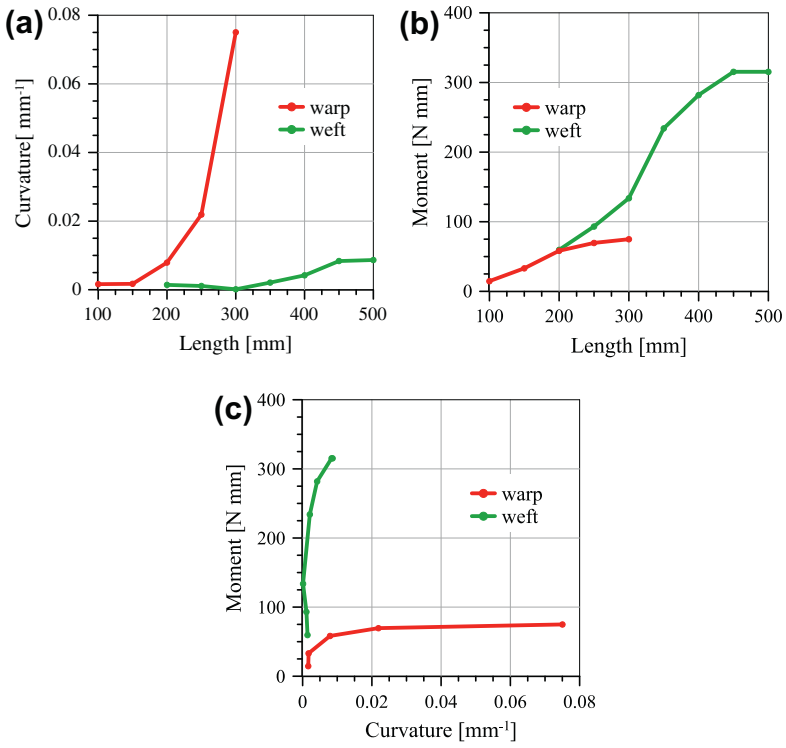

Fig. 6. Bending tests in warp and weft direction for the non-crimp 3D orthogonal weave preform. (a) Curvature vs. overhanging length; (b) bending moment vs. overhanging length; and (c) bending moment vs. curvature. (For interpretation of the references to colour in this figure legend, the reader is referred to the web version of this article.)

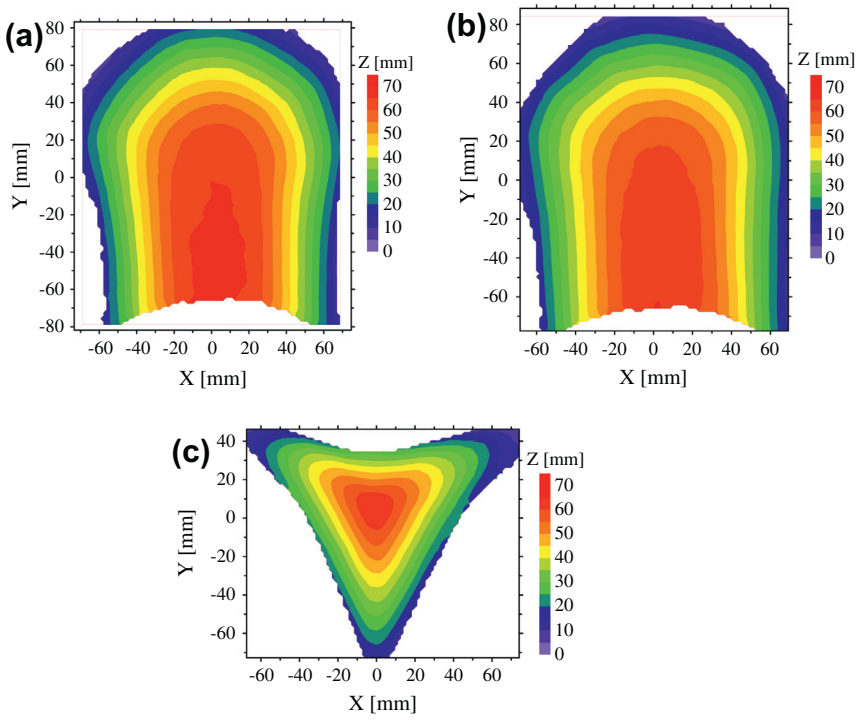

Fig. 7. Displacement distribution at the end of forming process: double-dome shape with (a) fabric yarn orientations 0°/90° and (b) fabric with yarn orientations ±45°; and (c) tetrahedral shape. (For interpretation of the references to colour in this figure legend, the reader is referred to the web version of this article.)

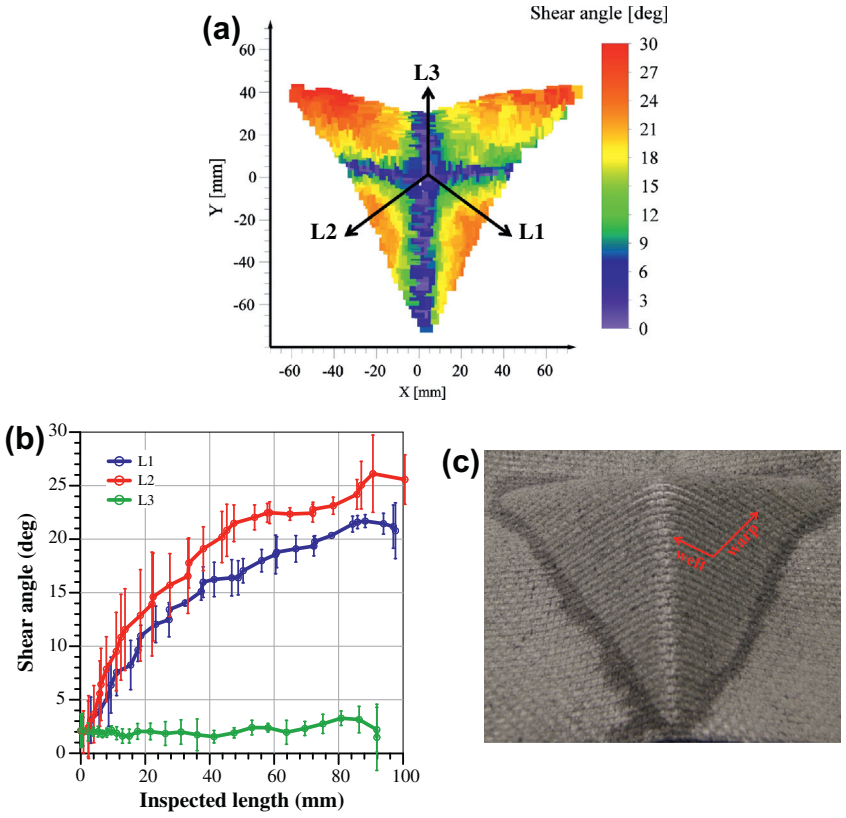

Fig. 8. Tetrahedral shape forming test. Shear angle distribution at the end of forming process: (a) on the 3D reinforcement surface; and (b) along paths L1, L2, L3 (error bars give the standard deviation of four tests). (c) Deformed shape of the 3D fabric at the end of the forming. (For interpretation of the references to colour in this figure legend, the reader is referred to the web version of this article.)

bending behaviour of other glass 3D textiles is not available in literature. The single layer 3D reinforcement reveals a higher bending stiffness in both yarn directions with respect to the considered carbon reinforcements. The high bending stiffness of the 3D glass reinforcement justifies the adopted forming set-up without blank holder.

The ratio of fabric bending per yarn to the yarn bending stiffness is studied in [41]. It is estimated, theoretically and derived from experimental data, to have values 2–2.5 for 2D woven fabrics with high crimp (up to ∼15%) and high cover factor, while for 2D fabrics with crimp below 2–3% the bending fabric-to-yarn ratio is close to 1. This ratio for the 3D glass fabrics studied here can be estimated for bending in the weft direction, having equal weft yarns. The bending rigidity of a weft tow is 1.025 N mm^2, hence the bending fabric-to-yarn ratio is close to 395. This value is much higher than the typical values for 2D woven fabrics, even with high crimp. This highlights the role of the fabric thickness and the strong connection of the layers with Z-yarns on the 3D fabric resistance to bending.

5. Forming of complex shapes

The measurement of the shear angle distribution on the preform is an important result of the experiments. It influences directly the permeability of the preform and therefore, the mechanical quality of the final composite component [3].

During forming a two-camera stereo vision system (see Fig. 3), acquire images at displacement increments of the punch of 0.167 mm. MatchID3D image correlation software allows extracting the coordinates of the points randomly distributed in the speckle pattern. The main benefit of this technique is the displacement measurement via a contactless method. One drawback could be the degradation of the pattern in the high deformed zones.

Being the shear deformation considered one of the primary deformation mechanisms in the forming of composite reinforcements [14], the local shear angle is here calculated by means of the 'grid method', presented in [42]. The grid consists of facets, made by spacing of points (i.e. step size in pixels), in the Area of Interest (AoI) analysed during the correlation. The adopted step size is 8 pixels.

For each recorded incremental position of the mould, DIC analysis provides the 3D displacement in the field of view of the cameras as coordinates of the facets vertexes (see Fig. 7). The post-processing of the recorded data allows evaluating the local shear angle at the scale level of the unit cell (meso-scale). An initial square set of 4×4 facets is considered having dimensions close to those of the unit cell $\approx 6 \times 6$ mm^2. The shear angle is the variation of the angle between two consecutive sides or diagonals of each set of facets according to the initial yarns direction in the un-deformed reinforcement.

5.1. Tetrahedral shape

The contour plot in Fig. 8a shows the map of the shear angle on the 3D reinforcement at the end of tetrahedral shape forming process. This complex shape deforms the 3D textile in such a way that the higher shear angle is lower than 27°, at the conclusion of the shaping. In addition, shear angles are detailed along some selected paths (lines L1, L2, L3 in Fig. 8a) on the deformed reinforcement. The average curves of the four forming tests are in Fig. 8b.

The shear angle distribution on the 3D reinforcement (see Fig. 8a and b) is similar to that observed and numerically predicted in [3] for the tetrahedral shape forming of an interlock carbon fabric (areal density 630 g/m^2). Furthermore, by comparing the graphs illustrated in Fig. 8 with the results reported in [3], it is possible to notice that both reinforcements show similar maximum value of the shear angle.

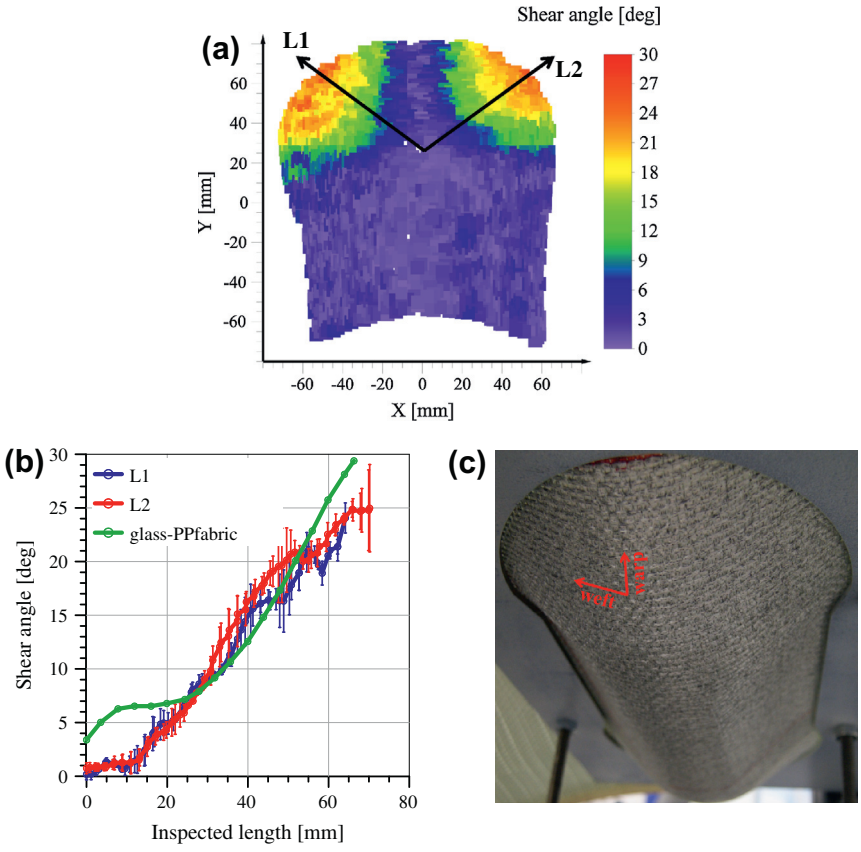

Fig. 9. Double-dome forming tests for fabric with yarn orientations 0°/90°. Shear angle distribution at the end of forming process: (a) on the 3D reinforcement surface; and (b) along paths L1, L2 (error bars give the standard deviation of three tests) and for the glass-PP fabric reported in [37]. (c) Deformed shape of the 3D fabric at the end of the forming. (For interpretation of the references to colour in this figure legend, the reader is referred to the web version of this article.)

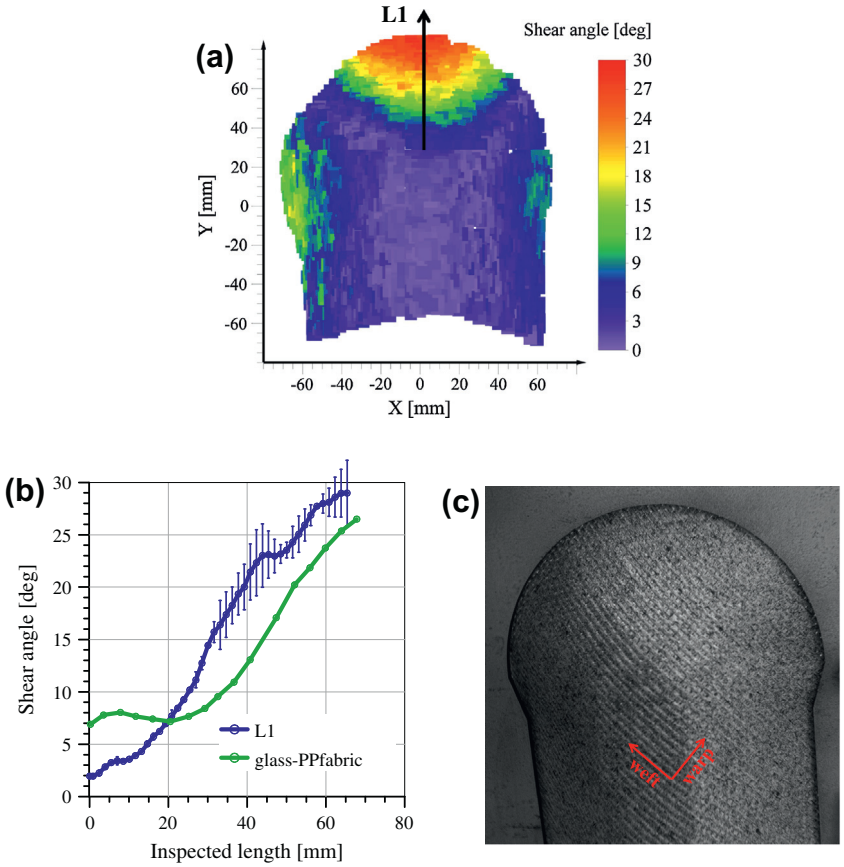

Fig. 10. Double-dome forming tests for fabric with yarn orientations ±45°. Shear angle distribution at the end of forming process: (a) on the 3D reinforcement surface; and (b) along the path L1 (error bars give the standard deviation of two tests) and for the glass-PP fabric reported in [37]. (c) Deformed shape of the 3D fabric at the end of the forming. (For interpretation of the references to colour in this figure legend, the reader is referred to the web version of this article.)

It is particularly interesting to notice the absence of wrinkles in the tetrahedral shape of the 3D reinforcement (see Fig. 8c). This observation confirms that the bending stiffness of the 3D textile is enough to avoid wrinkles and a blank holder is not necessary in the forming set-up.

5.2. Double-dome shape

The distributions of the shear angle on the reinforcement external surface at the end of the double-dome shape forming, for samples with yarn orientations of 0°/90° and ±45°, are depicted in Figs. 9a and 10a, respectively. Moreover, shear angles are extracted along paths which pass through the zones of greatest shear (lines L1 and L2 in Fig. 9a, and line L1 in Fig. 10a). The shear angle distribution along the selected paths is average of three specimens 0°/90° in Fig. 9b and average of two specimens ±45° in Fig. 10b.

The blanks oriented at 0°/90° show higher concentration of shear angle in the higher curvature zone (top right and left zones of picture in Fig. 9a). The maximum shear angle does not exceed about 25° for the reinforcement in the final shape. The blanks oriented at ±45° have the higher concentration of shear angle in the centre of the higher curvature zone and the maximum shear angle is lower than 30° (see Fig. 10).

The behaviour during forming of the 3D glass reinforcement is compared to double-dome experimental data of a twill 2/2 glass-PP fabric (areal density 1485 g/m^2), reported in [37]. The experimental set-up adopted in [37] consists of match tooling (male and female), while in the present work an open die is adopted to have a continuous observation of the forming process. The comparisons, in terms of shear angle distribution along lines passing through the zones of greatest shear are in Figs. 9b and 10b. It must be underlined that the double-dome mould shown in Fig. 3b is the same used in [37]; therefore, the same inspected paths are compared in Figs. 9b and 10b. Judging the data of Figs. 9b and 10b, the non-crimp 3D reinforcement has a behaviour similar to the twill 2/2 fabric with lower maximum shear angle in the 0°/90° configuration and higher maximum shear angle in the ±45° blank. The observed differences can be explained with the different deformation properties of the two reinforcements and the difference in forming tooling.

As for the tetrahedron shape, the single layer 3D reinforcement does not show relevant defects (e.g. wrinkles) during the double-dome forming for both the considered initial orientations of the yarns (Figs. 9c and 10c).

6. Conclusions

The experimental study presented in this paper is focused on the formability of a single layer non-crimp 3D orthogonal weave E-glass composite reinforcement, commercialized under trademark 3WEAVE® by 3Tex Inc. The experimental forming process was investigated with two complex shapes, i.e. double-dome and tetrahedron. The 3D digital image correlation technique allowed measuring the shear angle distribution on the reinforcement during shaping.

The most remarkable results of the investigation are:

– Bending tests in warp and weft direction revealed the higher out-of-plane stiffness of the 3D reinforcement in comparison to 2D textiles. These tests have pointed out the importance of the fabric bending stiffness, in preventing wrinkling onset during shaping processes.

– Experimental observations showed that the peculiar mechanical properties of the single layer non-crimp 3D orthogonal weave glass reinforcement are appropriate to generate the considered complex shapes without defects like wrinkles.

The obtained experimental results represent an important data set including information on the deformation behaviour of the considered 3D reinforcement during forming of complex three-dimensional shapes. These are very useful for the assessment of numerical modelling of shaping processes with such 3D reinforcement.

Acknowledgements

3Tex Inc. is acknowledged for manufacturing and supplying the non-crimp 3D orthogonal weave E-glass reinforcement (3WEAVE®). The research visit of J. Pazmino to K.U. Leuven was partially supported by INFUCOMP (FP7) project. The help of laboratory staff of the Department MTM – Bart Pelgrims – is acknowledged. The support and help in DIC computations by MatchID3D of Bart Van Mieghem and Pascal Lava is gratefully acknowledged.

References

[1] Long AC. Design and manufacture of textile composites. New York (USA): Woodhead Publishing Limited & CRC Press LLC; 2005.
[2] de Bilbao E, Soulat D, Hivet G, Gasser A. Experimental study of bending behaviour of reinforcements. Exp Mech 2010;50:333–51.
[3] Allaoui S, Boisse P, Chatel S, Hamila N, Hivet G, Soulat D, et al. Experimental and numerical analyses of textile reinforcement forming of a tetrahedral shape. Composites: Part A 2011;42:612–22.
[4] Bogdanovich AE, Mohamed MH. Three-dimensional reinforcement for composites. SAMPE J 2009;45:8–28.
[5] Long AC. Composites forming technologies. Woodhead Publishing Limited; 2007.
[6] Boisse P. Composite reinforcements for optimum performance. Woodhead Publishing Limited; 2011.
[7] Khan MA, Mabrouki T, Vidal-Sallè E, Boisse P. Numerical and experimental analyses of woven composite reinforcement forming using a hypoelastic behaviour. Application to the double-dome benchmark. J Mater Process Technol 2010;210:378–88.
[8] Zhu B, Yu TX, Zhang H, Tao XM. Experimental investigation of formability of commingled woven composite preform in stamping operation. Composites: Part B 2011;42:289–95.
[9] De Luycker E, Morestin F, Boisse P, Marsal D. Simulation of 3D interlock composite preforming. Compos Struct 2009;88:615–23.
[10] Charmetant A, Orliac JG, Vidal-Sallè E, Boisse P. Hyperelastic model for large deformation analyses of 3D interlock composite preforms. Compos Sci Technol 2012;72:1352–60.
[11] Karahan M, Lomov SV, Bogdanovich AE, Mungalov D, Verpoest I. Internal geometry evaluation of non-crimp 3D orthogonal woven carbon fabric composite. Composites: Part A 2010;41:1301–11.
[12] Desplentere F, Lomov SV, Woerdeman DL, Verpoest I, Wevers M, Bogdanovich A. Micro-CT characterization of variability in 3D textile architecture. Compos Sci Technol 2005;65:1920–30.
[13] Mc Clain M, Goering J. Stretch broken carbon fiber (SBCF) preforms: dry forming internal structural stiffeners. SAMPE J 2007;43(6):6–9.
[14] Potluri P, Parlak I, Ramgulam R, Sagar TV. Analysis of tow deformations in textile preforms subjected to forming forces. Compos Sci Technol 2006;66:297–305.
[15] Boisse P, Hamila N, Vidal-Sallè E, Dumont F. Simulation of wrinkling during textile composite reinforcement forming. Influence of tensile, in-plane shear and bending stiffnesses. Compos Sci Technol 2011;71:683–92.
[16] Carvelli V, Pazmino J, Lomov SV, Verpoest I. Deformability of a non-crimp 3D orthogonal weave E-glass composite reinforcement. Compos Sci Technol 2012;73:9–18.
[17] Pazmino J, Carvelli V, Lomov SV. Micro-CT analysis of the internal deformed geometry of a non-crimp 3D orthogonal weave E-glass composite reinforcement. Composites: Part B 2013. http://dx.doi.org/10.1016/j.compositesb.2013.11.024 [in print].
[18] Pazmino J, Carvelli V, Lomov SV, Van Mieghem B, Lava P. 3D digital image correlation measurements during shaping of a non-crimp 3D orthogonal woven E-glass reinforcement. Int J Mater Form 2013. http://dx.doi.org/10.1007/s12289-013-1139-6 [in print].
[19] Gatouillat S, Bareggi A, Vidal-Sallé E, Boisse P. Meso modelling for composite preform shaping – simulation of the loss of cohesion of the woven fibre network. Composites: Part A 2013;54:135–44.
[20] Peng X, Ding F. Validation of a non-orthogonal constitutive model for woven composite fabrics via hemispherical stamping simulation. Composites: Part A 2011;42:400–7.
[21] Carvelli V, Gramellini G, Lomov SV, Bogdanovich AE, Mungalov DD, Verpoest I. Fatigue behaviour of non-crimp 3D orthogonal weave and multi-layer plain weave E-glass reinforced composites. Compos Sci Technol 2010;70:2068–76.
[22] Lomov SV, Bogdanovich AE, Ivanov DS, Karahan M, Verpoest I. A comparative study of tensile properties of non-crimp 3D orthogonal weave and multilayer plain weave E-glass composites. Part1: Materials, methods and principal results. Composites: Part A 2009;40:1134–43.
[23] Ivanov DS, Lomov SV, Bogdanovich AE, Karahan M, Verpoest I. A comparative study of tensile properties of non-crimp 3D orthogonal weave and multi-layer plain weave E-glass composites. Part 2: Comprehensive experimental results. Composites: Part A 2009;40:1144–52.
[24] Mohamed MH, Zhang ZH. Method of forming variable cross-sectional shaped three-dimensional fabrics; 4 February 1992 US Patent 5085252.
[25] Bogdanovich AE. Advancements in manufacturing and applications of 3D woven preforms and composites. In Proceeding of 16th international conference on composite materials (ICCM 16). Kyoto-Japan; 2007.
[26] Hearle JWS, Amirbayat J. Analysis of drape by means of dimensionless groups. Text Res J 1986;56(12):727–33.
[27] Amirbayat J, Hearle JWS. The anatomy of buckling of textile fabrics: drape and conformability. J Text Inst 1989;80(1):51–69.
[28] Amirbayat J, Hearle JWS. The complex buckling of flexible sheet materials. Part I: Theoretical approach. Int J Mech Sci 1986;28(6):339–58.
[29] Amirbayat J, Hearle JWS. The complex buckling of flexible sheet materials. Part II: Experimental study of 3-fold buckling. Int J Mech Sci 1986;28(6):359–70.
[30] Gereke T, Döbrich O, Hübner M, Cherif C. Experimental and computational composite textile reinforcement forming: a review. Composites: Part A 2013;46:1–10.
[31] Peirce F. The geometry of cloth structure. J Text Inst 1937;28:45–96.
[32] ASTM, D1388-08. Standard test method for stiffness of fabrics. West Conshohocken (PA): American Society for Testing and Materials; 2012.
[33] Lomov SV, Verpoest I, Barburski M, Laperre J. Carbon composites based on multiaxial multiply stitched preforms. Part 2. KES-F characterisation of the deformability of the preforms at low loads. Composites: Part A 2003;34(4):359–70.
[34] Hamila N, Boisse P, Sabourin F, Brunet M. A semi-discrete shell finite element for textile composite reinforcement forming simulation. Int J Numer Methods Eng 2009;79:1443–66.
[35] Allaoui S, Launay J, Soulat D, Chatel S. Experimental tool of woven reinforcement forming. Int J Mater Form 2008;1:815–8.
[36] Sargent J, Chen J, Sherwood J, Cao J, Boisse P, Willems A, et al. Benchmark study of finite element models for simulating the thermostamping of woven-fabric reinforced composites. Int J Mater Form 2010;3(1):683–6.
[37] Willems A. Forming simulation of textile reinforced shell structures. PhD thesis, Katholieke Universiteit Leuven; 2008.
[38] Harrison P, Gomes R, Curado-Correia N. Press forming a 0/90 cross-ply advanced thermoplastic composite using the double-dome benchmark geometry. Composites: Part A 2013;54:56–69.
[39] MatchID – image correlation & material identification mechanics of materials, products & processes. <http://www.matchid.org/>.
[40] Sutton MA, Orteu JJ, Shreir HW. Image correlation for shape, motion and deformation measurements: basic concepts, theory and applications. Springer Science; 2009.
[41] Lomov SV, Truevtzev AV, Cassidy C. A predictive model for the fabric-to-yarn bending stiffness ratio of a plain-woven set fabric. Text Res J 2000;70(12):1088–96.
[42] Lomov SV, Boisse P, Deluycker E, Morestin F, Vanclooster K, Vandepitte D, et al. Full-field strain measurements in textile deformability studies. Composites: Part A 2008;38:1232–44.